Biochemical and Biophysical Research Communications 428 (2012) 239–244

Contents lists available at SciVerse ScienceDirect

Biochemical and Biophysical Research Communications

journal homepage: www.elsevier.com/locate/ybbrc

Cyanide binding to human plasma heme–hemopexin: A comparative study

Paolo Ascenzi [a,b,*], Loris Leboffe [b], Fabio Polticelli [c]

[a] Laboratorio Interdipartimentale di Microscopia Elettronica, Università Roma Tre, Roma, Italy
[b] Istituto Nazionale di Biostrutture e Biosistemi, Roma, Italy
[c] Dipartimento di Biologia, Università Roma Tre, Roma, Italy

ARTICLE INFO

Article history:
Received 28 September 2012
Available online 13 October 2012

Keywords:
Human heme–hemopexin
Cyanide binding
Thermodynamics
Kinetics
Molecular modeling

ABSTRACT

Hemopexin (HPX) displays a pivotal role in heme scavenging and delivery to the liver. In turn, heme–Fe–hemopexin (HPX–heme–Fe) displays heme-based spectroscopic and reactivity properties. Here, kinetics and thermodynamics of cyanide binding to ferric and ferrous hexa-coordinate human plasma HPX–heme–Fe (HHPX–heme–Fe(III) and HHPX–heme–Fe(II), respectively), and for the dithionite-mediated reduction of the HHPX–heme–Fe(III)–cyanide complex, at pH 7.4 and 20.0 °C, are reported. Values of thermodynamic and kinetic parameters for cyanide binding to HHPX–heme–Fe(III) and HHPX–heme–Fe(II) are $K = (4.1 \pm 0.4) \times 10^{-6}$ M, $k_{on} = (6.9 \pm 0.5) \times 10^{1}$ M^{-1} s^{-1}, and $k_{off} = 2.8 \times 10^{-4}$ s^{-1}; and $H = (6 \pm 1) \times 10^{-1}$ M, $h_{on} = 1.2 \times 10^{-1}$ M^{-1} s^{-1}, and $h_{off} = (7.1 \pm 0.8) \times 10^{-2}$ s^{-1}, respectively. The value of the rate constant for the dithionite-mediated reduction of the HHPX–heme–Fe(III)–cyanide complex is $l = 8.9 \pm 0.8$ $M^{-1/2}$ s^{-1}. HHPX–heme–Fe reactivity is modulated by proton acceptor/donor amino acid residue(s) (*e.g.*, His236) assisting the deprotonation and protonation of the incoming and outgoing ligand, respectively.

1. Introduction

Heme scavenging by plasma proteins (*i.e.*, high and low density lipoproteins (HDL and LDL, respectively), serum albumin (SA), and hemopexin (HPX)) provides protection against heme oxidative damage, limits the access of pathogens to heme, and contributes to iron homeostasis. In particular, during the first seconds after its appearance in plasma, most of the heme binds to HDL and LDL. Then, the heme moves from HDL and LDL to SA. Afterwards, the heme transits from SA to HPX, that releases it into hepatic parenchymal cells after internalization of the heme–Fe–hemopexin complex (HPX–heme–Fe) by receptor-mediated endocytosis. Then, HPX is released intact into the bloodstream and the heme is catabolyzed or used for the synthesis of hemoproteins or exported to bile canaliculi [1–8].

In turn, plasma proteins display transient heme-based ligand binding and (pseudo-)enzymatic properties, representing cases for "chronosteric effects". In particular, ferrous SA-heme, HPX–heme–Fe, HDL–heme–Fe, and LDL–heme–Fe bind reversibly CO and/or NO, however O_2 induces fast oxidation of the heme–Fe(II) atom. Moreover, NO induces the reductive nitrosylation of ferric SA–heme–Fe and HPX–heme–Fe. Furthermore, SA–heme–Fe and HPX–heme–Fe facilitate scavenging of reactive nitrogen and oxygen species. Lastly, NO appears to modulate heme binding to HPX, in turn HPX–heme–Fe may play a key role in the NO homeostasis [5–8].

Here, cyanide binding properties of ferric and ferrous human HPX-heme (HHPX–heme–Fe(III) and HHPX–heme–Fe(II), respectively) are reported and examined in parallel with those of related systems (the term cyanide refers to all forms of HCN/CN^- present in the buffered aqueous solution). Despite the different heme distal site structures and ligand interactions, values of kinetic and thermodynamic parameters for cyanide binding to most ferric (non)vertebrate heme-proteins are similar, being mainly influenced by the presence in the heme pocket of proton acceptor/donor group(s) (*e.g.*, His236 in human hemopexin (HHPX)) assisting the deprotonation and the protonation of the incoming and outgoing ligand, respectively.

2. Materials

HHPX and hemin [iron(III)–protoporphyrin(IX)] were obtained from Sigma–Aldrich (St. Louis, MO, USA). The concentration of

Abbreviations: Hb, hemoglobin; HDL, high density lipoprotein; HPX, hemopexin; HPX–heme–Fe, heme–Fe–hemopexin; HHPX, human HPX; HHPX–heme–Fe, human HPX–heme–Fe; HHPX–heme–Fe(III), ferric HHPX–heme–Fe; HHPX–heme–Fe(II), ferrous HHPX–heme–Fe; LDL, low density lipoprotein; legHb, leghemoglobin; Mb, myoglobin; trHb, truncated hemoglobin; Ngb, neuroglobin; *Ce*-trHbN, *Chlamydomonas eugametos* truncated hemoglobin N; *Mt*-trHbN, *Mycobacterium tuberculosis* truncated hemoglobin N; *Mt*-trHbO, *Mycobacterium tuberculosis* truncated hemoglobin O; *Cj*-trHbP, *Campylobacter jejuni* truncated hemoglobin P; SA, serum albumin.

* Corresponding author. Address: Laboratorio Interdipartimentale di Microscopia Elettronica, Via della Vasca Navale 79, I-00146 Roma, Italy.
E-mail address: ascenzi@uniroma3.it (P. Ascenzi).

0006-291X/$ - see front matter © 2012 Elsevier Inc. All rights reserved.
http://dx.doi.org/10.1016/j.bbrc.2012.10.027

HHPX was determined spectrophotometrically at 414 nm, $E_{1cm}^{1\%} = 23.0$ [9]. The HHPX–heme–Fe(III) stock solution (2.0×10^{-5} M) was prepared by adding 1.25 molar excess of the HHPX solution (2.0×10^{-5} M) to the heme–Fe(III) solution (1.6×10^{-5} M), at pH 7.4 (1.0×10^{-1} M phosphate buffer) and 20.0 °C. Under these conditions, no free heme–Fe(III) is present in solution; in fact, the value of the dissociation equilibrium constant for heme binding to HHPX is $<10^{-9}$ M [5–7]. HHPX–heme–Fe(II) was prepared by adding sodium dithionite (1.0×10^{-2} M) to the HHPX–heme–Fe(III) solution [9]. All the other chemicals were from Merck AG (Darmstadt, Germany) or Carlo Erba Reagenti (Milano, Italy). All products were of analytical or reagent grade and were used without further purification.

3. Methods

3.1. Thermodynamics and kinetics of cyanide binding to HHPX–heme–Fe(III)

Thermodynamics and kinetics of cyanide binding to HHPX–heme–Fe(III) was monitored spectrophotometrically between 360 and 460 nm, and analyzed according to the minimum reaction mechanism depicted by Scheme 1 [10–12].

The value of the dissociation equilibrium constant for cyanide binding to HHPX–heme–Fe(III) (*i.e.*, $K = k_{off}/k_{on}$) was determined from the dependence of the molar fraction of the HHPX–heme–Fe(III)–cyanide complex (*i.e.*, Y) on the ligand concentration (*i.e.*, [cyanide]), according to Eq. (1) [12]:

$$Y = [\text{cyanide}]/(K + [\text{cyanide}]) \quad (1)$$

The HHPX–heme–Fe(III) concentration was 2.0×10^{-6} M. The free cyanide concentration ranged between 1.0×10^{-6} M and 4.0×10^{-5} M. The equilibration time ranged between 1 and 24 h.

The value of the second-order rate constant for cyanide binding to HHPX–heme–Fe(III) (*i.e.*, k_{on}; Scheme 1) was determined from the dependence of the pseudo first-order rate constant for HHPX–heme–Fe(III) ligation (*i.e.*, k_{obs}) on [cyanide], according to Eqs (2) and (3) [12]:

$$\text{HHPX-heme-Fe(III)} + \text{cyanide} \underset{k_{off}}{\overset{k_{on}}{\rightleftharpoons}} \text{HHPX-heme-Fe(III)-cyanide}$$

Scheme 1. Cyanide binding to HHPX–heme–Fe(III).

$$\text{HHPX-heme-Fe(II)} + \text{cyanide} \underset{h_{off}}{\overset{h_{on}}{\rightleftharpoons}} \text{HHPX-heme-Fe(II)-cyanide}$$

Scheme 2. Cyanide binding to HHPX–heme–Fe(II).

$$[\text{HHPX—heme—Fe(III)—cyanide}]_t = [\text{HHPX—heme—Fe(III)}]_i \times (1 - e^{-kobs \times t}) \quad (2)$$

$$k_{obs} = k_{on} \times [\text{cyanide}] \quad (3)$$

The HHPX–heme–Fe(III) concentration was 5.0×10^{-6} M. The cyanide concentration ranged between 1.0×10^{-3} M and 1.0×10^{-2} M.

The value of the first-order rate constant for cyanide dissociation from the HHPX–heme–Fe(III)–cyanide complex (*i.e.*, k_{off}; Scheme 1) was calculated from values of K and k_{on}, according to Eq. (4) [12]:

$$k_{off} = K \times k_{on} \quad (4)$$

3.2. Thermodynamics and kinetics of cyanide binding to HHPX–heme–Fe(II)

Thermodynamics and kinetics of cyanide binding to HHPX–heme–Fe(II) was monitored spectrophotometrically between 360 and 460 nm, and analyzed according to the minimum reaction mechanism depicted by Scheme 2 [10,12].

The value of the dissociation equilibrium constant for cyanide binding to HHPX–heme–Fe(II) (*i.e.*, $H = h_{off}/h_{on}$) was determined from the dependence of the molar fraction of the HHPX–heme–Fe(II)–cyanide complex (*i.e.*, α) on [cyanide], according to Eq. (5) [12]:

$$\alpha = [\text{cyanide}]/(H + [\text{cyanide}]) \quad (5)$$

The HHPX–heme–Fe(II) concentration was between 5×10^{-6} M. The cyanide concentration ranged between 1.0×10^{-1} M and 2.0 M. The equilibration time ranged between 30 and 500 s.

Kinetics of the dithionite-mediated reduction of the HHPX–heme–Fe(III)–cyanide complex and of cyanide dissociation from the HHPX–heme–Fe(II)–cyanide complex were analyzed according to the minimum reaction mechanism depicted by Scheme 3 [10].

Values of the pseudo first-order rate constant for the dithionite-mediated reduction of the HHPX–heme–Fe(III)–cyanide complex (*i.e.*, l_{obs}) and of the first-order rate constant for cyanide dissociation from the HHPX–heme–Fe(II)–cyanide complex (h_{off}) were determined according to Eqs. (6)–(8) treating both reactions as irreversible first-order processes [10]:

$$[\text{HHPX—heme—Fe(III)—cyanide}]_t = [\text{HHPX—heme—Fe(III)—cyanide}]_i \times e^{-lobs \times t} \quad (6)$$

$$[\text{HHPX—heme—Fe(II)—cyanide}]_t = [\text{HHPX—heme—Fe(III)—cyanide}]_i \times l_{obs} \times ((e^{-lobs/(hoff-lobs)}) + (e^{-hoff/(lobs-hoff)})) \quad (7)$$

$$[\text{HHPX—heme—Fe(II)}]_t = [\text{HHPX—heme—Fe(III)—cyanide}]_i - ([\text{HHPX—heme—Fe(III)—cyanide}]_t + [\text{HHPX—heme—Fe(II)—cyanide}]_t) \quad (8)$$

$$\text{HHPX-heme-Fe(III)-cyanide} + \text{dithionite} \xrightarrow{l_{obs}} \text{HHPX-heme-Fe(II)-cyanide} \xrightarrow{h_{off}} \text{HHPX-heme-Fe(II)} + \text{cyanide}$$

Scheme 3. Dithionite-mediated reduction of HHPX–heme–Fe(III)–cyanide.

Since the HHPX–heme–Fe(III)–cyanide reducing species is sulfur dioxide (*i.e.*, SO_2^-), a dissociation product of dithionite (*i.e.*, $Na_2S_2O_4$) [13], the value of l (of order lower than two) has been determined from the linear dependence of l_{obs} on the square root of dithionite concentration (*i.e.*, [dithionite]$^{1/2}$), under pseudo-first-order conditions (*i.e.*, [dithionite] > [HHPX–heme–Fe(III)–cyanide]), according to Eq. (9) [10,14]:

$$l_{obs} = l \times [\text{dithionite}]^{1/2} \quad (9)$$

The final HHPX–heme–Fe(II) concentration was 5×10^{-6} M. The final cyanide concentration was 1.0×10^{-3} M, and the final dithionite concentration ranged between 1.0×10^{-3} M and 1.0×10^{-1} M.

The value of the second-order rate constant for cyanide binding to HHPX–heme–Fe(II) was calculated according to Eq. (10) [12]:

$$h_{on} = h_{off}/H \quad (10)$$

All data (obtained at pH 7.0, 5.0×10^{-2} M phosphate buffer, and 20.0 °C) were determined at least in quadruplicate. Data analysis was performed with the program MATLAB 7.0 (MathWorks, Inc., South Natick, MA, USA).

3.3. Molecular modeling of HHPX–heme–Fe(III)

The structural model of HHPX–heme–Fe(III) has been obtained by homology modeling using the three dimensional structure of the highly homologous rabbit HPX–heme–Fe(III) (PDB code: 1QHU [15]). In detail, the template protein displaying the highest similarity with HHPX was retrieved through a BLAST [16] search against the PDB amino acid sequence database using the HHPX sequence coded GI 184497 as a bait. The BLAST *E*-value for the rabbit protein was 0.0, given the extremely high sequence similarity between the two proteins, and the two sequences align over their entire length.

Based on this alignment, the molecular model of HHPX–heme–Fe(III) has been built using the program NEST [17], a fast model building program that applies an "artificial evolution" algorithm to construct a model from a given template and alignment. The NEST option *tune 2* was used to refine the alignment avoiding the unlikely occurrence of insertions and deletions within template secondary structure elements.

4. Results

Addition of cyanide to the HHPX–heme–Fe(III) solution causes a shift in the maximum of the optical absorption spectrum in the Soret band from 415 nm, *i.e.* HHPX–heme–Fe(III), to 421 nm, *i.e.* HHPX–heme–Fe(III)–cyanide.

As shown in Fig. 1 (panel A), cyanide binding to HHPX–heme–Fe(III) follows a simple equilibrium (Scheme 1 and Eq. (1)), the value of K is $(4.1 \pm 0.4) \times 10^{-6}$ M (Table 1). As expected for simple systems [18], the value of the Hill coefficient n for cyanide binding to HPX–heme–Fe(III) is 0.99 ± 0.02.

Over the whole cyanide concentration range explored (from 1.0×10^{-3} M to 1.0×10^{-2} M), the time course for cyanide binding to HHPX–heme–Fe(III) corresponds to a single exponential decay for more than 95% of its course between 360 and 460 nm (Eq. (2) and Fig. 1, panel B). Values of k_{obs} for cyanide binding to HHPX–heme–Fe(III) are wavelength-independent at fixed cyanide concentration. As shown in Fig. 1 (panel C), values of k_{obs} for cyanide binding to HHPX–heme–Fe(III) increase linearly with the ligand concentration (Scheme 1 and Eq. (3)), with a y-intercept close to 0, indicating $k_{off} \leqslant 1 \times 10^{-2}$ s^{-1}; the slope of the plot of k_{obs} versus [cyanide] corresponds to $k_{on} = (6.9 \pm 0.5) \times 10^1$ M^{-1} s^{-1} (Table 1).

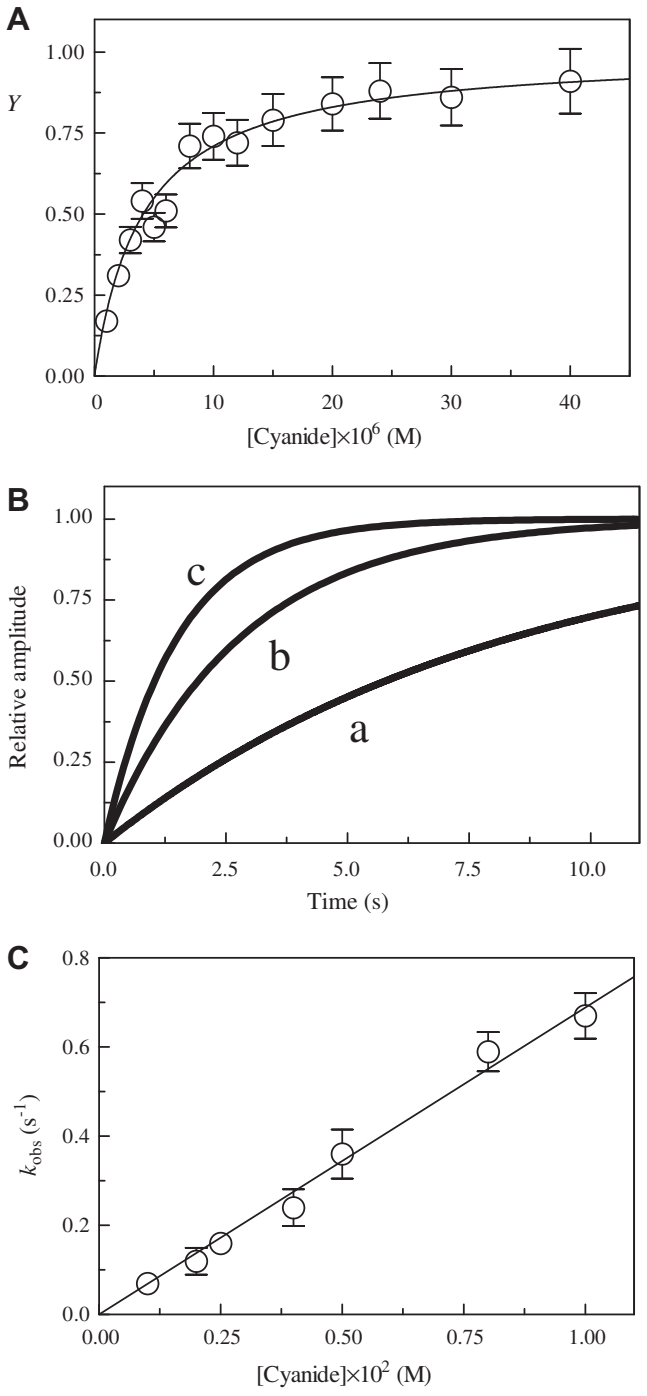

Fig. 1. Cyanide binding to HHPX–heme–Fe(III), at pH 7.0 and 20.0 °C. (Panel A) Ligand binding isotherm for cyanide association to HHPX–heme–Fe(III). The continuous line was calculated according to Eq. (1) with $K = (4.1 \pm 0.4) \times 10^{-6}$ M. (Panel B) Normalized averaged time courses for cyanide binding to HHPX–heme–Fe(III). The cyanide concentration was 2.0×10^{-3} M (trace a), 5.0×10^{-3} M (trace b), and 1.0×10^{-2} M (trace c). The time course analysis according to Eq. (2) yielded the following values of $k_{obs} = 1.2 \times 10^{-1}$ s^{-1} (trace a), 3.6×10^{-1} s^{-1} (trace b), and 6.7×10^{-1} s^{-1} (trace c). (Panel C) Dependence of the pseudo-first-order rate constant k_{obs} for cyanide binding to HHPX–heme–Fe(III) on the ligand concentration (*i.e.*, [cyanide]). The continuous line was calculated according to Eq. (3) with $k_{on} = (6.9 \pm 0.5) \times 10^1$ M^{-1} s^{-1}.

From values of k_{on} and K, the value of k_{off} for cyanide dissociation from the HHPX–heme–Fe(III)–cyanide complex (= 2.8×10^{-4} s^{-1}) was calculated according to Eq. (4) (Table 1).

Addition of cyanide to the HHPX–heme–Fe(II) solution causes a shift in the maximum of the optical absorption spectrum in the

Table 1
Values of kinetic and thermodynamic parameters for cyanide binding to ferric and ferrous monomeric heme-proteins as well as for dithionite-mediated reduction of the heme–Fe(III)–cyanide complexes[a].

(Non)vertebrate globin	Fe(III)			Fe(II)			$l(M^{1/2}s^{-1})$
	$k_{on}(M^{-1}s^{-1})$	$k_{off}(s^{-1})$	K (M)	$h_{on}(M^{-1}s^{-1})$	$h_{off}(s^{-1})$	H (M)	
Ce-trHbN[b]	4.6×10^{2}	n.d.	n.d.	n.d.	1.6×10^{-2}	n.d.	3.5
Mt-trHbN[c]	3.8×10^{2}	6.8×10^{-4}	1.8×10^{-6}	5.0×10^{-2}	1.3×10^{-2}	2.4×10^{-1}	3.1
Mt-trHbO[c]	3.2×10^{2}	3.5×10^{-4}	1.1×10^{-6}	8.5×10^{-2}	1.3×10^{-2}	1.6×10^{-1}	2.8
Cj-trHbP[d]	$>2 \times 10^{4}$	$>2 \times 10^{-4}$	5.8×10^{-9}	3.3×10^{3}	5.0×10^{-3}	1.2×10^{-6}	3.5
Soybean legHb[e]	6.9×10^{2}	n.d.	n.d.	n.d.	n.d.	n.d.	n.d.
Drosophila melanogaster Hb 1[f]	1.8×10^{2}	n.d.	n.d.	n.d.	n.d.	n.d.	n.d.
Glycera dibranchiata Hb II[g]	4.9×10^{-1}	n.d.	n.d.	n.d.	n.d.	n.d.	n.d.
Aplysia limacina Mb[h]	2.0×10^{2}	n.d.	n.d.	n.d.	2.2×10^{-2}	n.d.	$>1 \times 10^{2}$
Sperm whale Mb[i]	1.8×10^{2}[e]	8.0×10^{-4}[e]	4.3×10^{-6}	n.d.	2.1×10^{-2}[f]	4.0×10^{-1}[g]	4.4[f]
Horse heart Mb[J]	1.7×10^{2}[h]	3.0×10^{-3}	1.8×10^{-5}[h]	2.5[i]	1.5×10^{-1}[J]	4.0×10^{-1}[i]	8.0×10^{1}
Human Ngb (open conformation)[k]	1.7	n.d.	n.d.	n.d.	n.d.	n.d.	n.d.
(closed conformation)[k]	3.7×10^{-1}	n.d.	n.d.	n.d.	n.d.	n.d.	n.d.
HHPX–heme–Fe[l]	6.9×10^{1}	2.8×10^{-4}	4.1×10^{-6}	1.2×10^{-1}	7.1×10^{-2}	6.0×10^{-1}	8.9
Horseradish peroxidase[m]	9.0×10^{4}	2.8×10^{-1}	2.4×10^{-6}	2.9×10^{1}	2.5×10^{-2}	5.0×10^{-4}	n.d.
Horse heart cytochrome *c*[n]	5.1×10^{-2}	4.9×10^{-3}	2.5×10^{-4}	n.d.	n.d.	$>1 \times 10^{1}$	n.d.

n.d., not determined.
[a] Values of kinetic and thermodynamic parameters were obtained between pH 6.0 and 9.3, and between 20 and 25 °C.
[b] From [10].
[c] From [10,12].
[d] From [10,12].
[e] From [33].
[f] From [11].
[g] From [24].
[h] From [34,35].
[i] From [35,36].
[J] From [18,31,37].
[k] From [27].
[l] Present study.
[m] From [38,39].
[n] From [28,29].

Soret band from 429 nm, *i.e.* HHPX–heme–Fe(II), to 421 nm, *i.e.* HHPX–heme–Fe(II)–cyanide.

As shown in Fig. 2 (panel A), cyanide binding to HHPX–heme–Fe(II) follows a simple equilibrium (Scheme 2 and Eq. (5)), the value of H is $(6.0 \pm 1) \times 10^{-1}$ M (Table 1). As expected for simple systems [18], the value of the Hill coefficient n for cyanide binding to HHPX–heme–Fe(II) is 1.01 ± 0.02.

Addition of dithionite to the HHPX–heme–Fe(III)–cyanide solution causes a shift in the maximum of the optical absorption spectrum in the Soret band from 421 nm, *i.e.* HHPX–heme–Fe(III)–cyanide, to 433 nm, *i.e.* HHPX–heme–Fe(II)–cyanide. Then, the maximum of the optical absorption spectrum in the Soret band of HHPX–heme–Fe(II)–cyanide moves from 433 nm to 429 nm, *i.e.* HHPX–heme–Fe(II). Both processes correspond to a single exponential decay for more than 95% of their courses.

The reaction of HHPX–heme–Fe(III)–cyanide with dithionite conforms to the minimum two-step sequential reaction mechanism depicted in Scheme 3 (Fig. 2, panel B; Eqs. (6)–(8)). The first reaction is the reduction of HHPX–heme–Fe(III)–cyanide driven by dithionite. As demonstrated by the linear dependence of l_{obs} on the square root of dithionite concentration (Fig. 2, panel C; Eq. (9)), sulfur dioxide (a dissociation product of dithionite) is the reducing species [13]. The second reaction conforms to the irreversible monomolecular decay of the HHPX–heme–Fe(II)–cyanide reaction intermediate into HHPX–heme–Fe(II) and cyanide. Remarkably, values of h_{off} are independent of the dithionite concentration (Fig. 2, panel B); the average value of h_{off} is $(7.1 \pm 0.8) \times 10^{-2}$ s^{-1}. The analysis of the absorption changes between 360 and 460 nm according to Scheme 3 shows that HHPX–heme–Fe(II)–cyanide and HHPX–heme–Fe(II) are the intermediate and the final species, respectively. Indeed: (*i*) the time course for the buildup of the intermediate species HHPX–heme–Fe(II)–cyanide is a simple dithionite-dependent step; (*ii*) the decay of HHPX–heme–Fe(II)–cyanide into HHPX–heme–Fe(II) and cyanide is a simple dithionite-independent irreversible process; and (*iii*) static and kinetic absorption spectra of HHPX–heme–Fe(II)–cyanide and HHPX–heme–Fe(II) match each other very well.

From values of and H and h_{off}, the value of h_{on} for cyanide binding to HHPX–heme–Fe(III) (=1.2×10^{-1} M^{-1} s^{-1}) was calculated according to Eq. (10) (Table 1).

5. Discussion

Cyanide represents a valuable diatomic ligand model of heme-proteins being isosteric and isoelectronic with the diatomic carbon monoxide heme–Fe(II) ligand. Moreover, cyanide is one of the few ligands that is able to bind both ferric and ferrous heme-proteins though with different thermodynamic and kinetic parameters [18–20]. In fact, The cyanide derivative of ferric monomeric heme-proteins is very stable, values of K, k_{on} and k_{off} ranging between 5.8×10^{-9} M and 2.5×10^{-4} M, 5.1×10^{-2} M^{-1} s^{-1} and $\geqslant 2 \times 10^{4}$ M^{-1} s^{-1}, and $\geqslant 2 \times 10^{-4}$ s^{-1} and 2.8×10^{-1} s^{-1}, respectively. On the other hand, the cyanide reactivity towards ferrous monomeric heme-proteins is lower, values of H, h_{on}, and h_{off} ranging between 1.2×10^{-6} M and $>1 \times 10^{1}$ M, 5.0×10^{-2} M^{-1} s^{-1} and 3.3×10^{3} M^{-1} s^{-1}, and 5.0×10^{-3} s^{-1} and 1.5×10^{-1} s^{-1}, respectively (Table 1).

In most ferric heme-proteins, cyanide binding is mainly influenced by the presence in the heme pocket of proton acceptor and donor group(s) assisting the deprotonation and protonation of the incoming and outgoing ligand, respectively, rather than the heme–Fe atom coordination geometry. In fact, most six- and five-coordinate heme-proteins, *e.g.* HHPX–heme–Fe (present study) and *Aplysia limacina* myoglobin (Mb) [21,22], respectively (Fig. 3), display similar kinetic and thermodynamic parameters for cyanide binding (Table 1). Interestingly, the heme–Fe binding

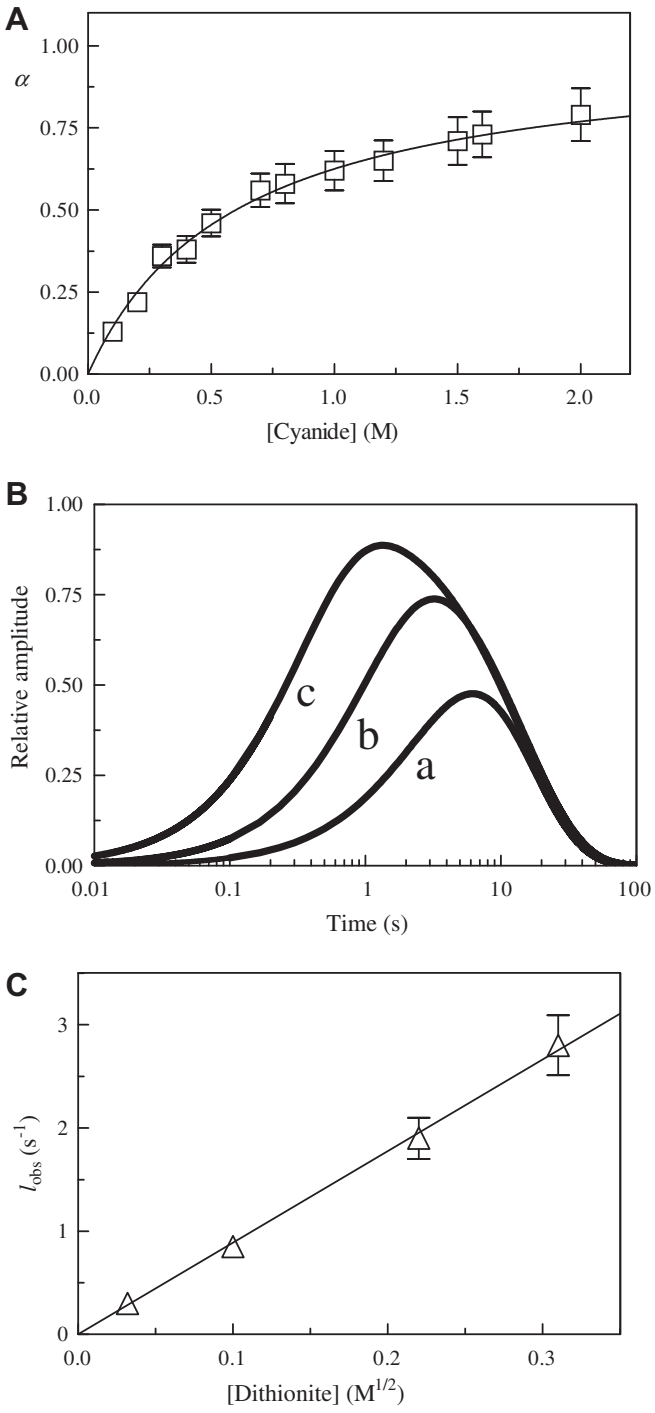

Fig. 2. Cyanide binding to HHPX–heme–Fe(II), at pH 7.0 and 20.0 °C. (Panel A) Ligand binding isotherm for cyanide association to HHPX–heme–Fe(II). The continuous line was calculated according to Eq. (5) with $H = (6 \pm 1) \times 10^{-1}$ M. (Panel B) Normalized averaged time courses for dithionite-mediated reduction of HHPX–heme–Fe(III)–cyanide. The dithionite concentration was 1.0×10^{-3} M (trace a), 1.0×10^{-2} M (trace b), and 1.0×10^{-1} M (trace c). The time course analysis according to Eqs. (6)–(8) yielded the following values of $l_{obs} = 3.0 \times 10^{-1}$ s^{-1} and $h_{off} = 7.4 \times 10^{-2}$ s^{-1} (trace a), $l_{obs} = 8.5 \times 10^{-1}$ s^{-1} and $h_{off} = 6.8 \times 10^{-2}$ s^{-1} (trace b), and $l_{obs} = 2.8$ s^{-1} and $h_{off} = 7.0 \times 10^{-2}$ s^{-1} (trace c). (Panel C) Dependence of the pseudo-first-order rate constant l_{obs} for dithionite-mediated reduction of HHPX–heme–Fe(III)–cyanide on dithionite concentration (*i.e.*, [dithionite]). The continuous line was calculated according to Eq. (9) with $l = 8.9 \pm 0.8$ $M^{-1/2}$ s^{-1}.

pocket of HHPX is formed by two similar four-bladed beta-propeller domains connected by an interdomain linker ([15] and Fig. 1 SM); on the other hand, *Aplysia limacina* Mb displays the classical globin fold [22,23]. Thus, the dissociation of the sixth heme–Fe

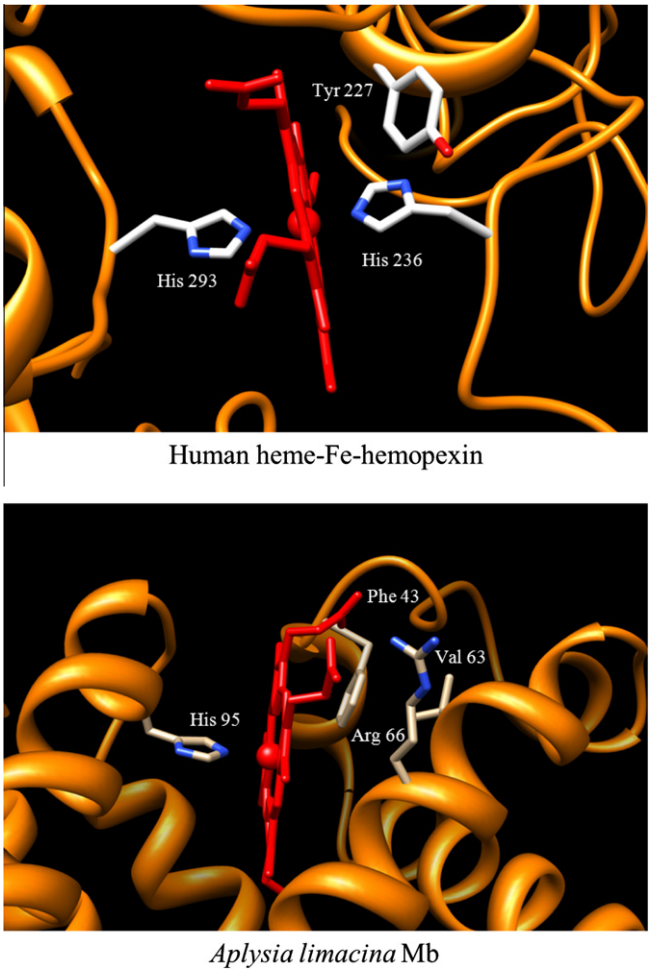

Fig. 3. View of the heme distal pocket of six-coordinate HHPX–heme–Fe(III) (present study) and five-coordinate *A. limacina* Mb(III) (Protein Data Bank code: 1MBA [22]), displaying part of the surrounding protein structure (ribbon), the heme–Fe(III) group (red), and key residues surrounding the heme–Fe(III) group. The three-dimensional model of HHPX–heme–Fe(III) has been built by homology modeling using the three-dimensional structure of rabbit HPX–heme–Fe(III) as a template (PDB code: 1QHU [15]). Both pictures have been drawn with program UCSF Chimera [40]. (For interpretation of the references to color in this figure legend, the reader is referred to the web version of this article.)

distal ligand (*e.g.*, His236 in HHPX–heme–Fe [15]) is not rate limiting in cyanide binding. Remarkably, the role of proton acceptor and donor group(s) in modulating cyanide binding to most heme-proteins is in agreement with: (*i*) the very slow kinetics of cyanide binding to five-coordinate ferric *Glycera dibranchiata* monomeric hemoglobin (Hb) II lacking heme distal site residue(s) capable of catalyzing proton exchange [24], and (*ii*) the effects shown by changes in the polarity of the heme distal pocket of mutated ferric human, pig, and sperm whale Mbs [25].

On the other hand, values of kinetic and thermodynamic parameters for cyanide binding to ferric *Campylobacter jejuni* truncated haemoglobin P (*Cj*-trHbP), horseradish peroxidase, human neuroglobin (Ngb), and horse heart cytochrome *c* mainly reflect the geometry of the heme–Fe pocket and/or the conformational transition(s) accompanying ligand binding. In fact, the high reactivity of *Cj*-trHbP towards cyanide (Table 1) has been attributed to the peculiar heme distal pocket geometry which is characterized by the presence of PheCD1, HisE7, IleE11, and TrpG8 residues [12]. The reactivity of horseradish peroxidase towards cyanide (Table 1) may reflect the geometry of the heme pocket tailored for O_2 chemistry rather than for O_2 transport [26]. The slow biphasic kinetics of

cyanide binding to six-coordinate human Ngb (Table 1) does not appear to be limited by the cleavage of the heme–Fe–HisE7 bond, but could reflect the presence of two distinct conformations of the protein (open and closed) in which the heme pocket is more or less accessible to exogenous ligands [27]. The very low reactivity of six-coordinate horse heart cytochrome *c* for cyanide (Table 1) has been attributed to the heme–Fe–Met80 bond strength and/or the flexibility of the heme–Fe pocket [28,29]. Accordingly, the reactivity towards cyanide of ferric five-coordinate horse heart carboxymethylated cytochrome *c* is higher than that of the native protein [28,30].

Lastly, values of the rate constant for dithionite-mediated reduction of the cyanide derivative of ferric monomeric heme-proteins (*i.e.*, *l*) range between 2.8 $M^{1/2}\,s^{-1}$ and $\geqslant 1 \times 10^2\,M^{1/2}\,s^{-1}$ (Table 1), reflecting the different ability of monomeric heme-proteins to yield productive complex(es) with either dithionite or with its byproduct SO_2^- [31].

As a whole, present data indicate that heme binding to HPX, that is crucial for the macrocycle scavenging, confers to HPX globin-like spectroscopic and reactivity properties. Since these features depend on the transient protein–ligand interaction(s), they have been called "chronosteric effects" [5,8,32].

Acknowledgments

Dr. Loris Leboffe is supported by a grant from the National Institute of Biostructures and Biosystems (INBB) of Italy. Part of this study was supported by a grant of University Roma Tre (Roma, Italy, CLAR-2011) to P.A.

Appendix A. Supplementary data

Supplementary data associated with this article can be found, in the online version, at http://dx.doi.org/10.1016/j.bbrc.2012.10.027.

References

[1] Y.I. Miller, N. Shaklai, Kinetics of hemin distribution in plasma reveals its role in lipoprotein oxidation, Biochim. Biophys. Acta 1454 (1999) 153–164.
[2] M.E. Conrad, J.N. Umbreit, Pathways of iron absorption, Blood Cells Mol. Dis. 29 (2002) 336–355.
[3] P. Ascenzi, M. Fasano, Heme-hemopexin: a "chronosteric" heme-protein, IUBMB Life 59 (2007) 700–708.
[4] V. Hvidberg, M.B. Maniecki, C. Jacobsen, P. Hojrup, H.J. Moller, S.K. Moestrup, Identification of the receptor scavenging hemopexin-heme complexes, Blood 106 (2005) 2572–2579.
[5] P. Ascenzi, A. Bocedi, P. Visca, F. Altruda, E. Tolosano, T. Beringhelli, M. Fasano, Hemoglobin and heme scavenging, IUBMB Life 57 (2005) 749–759.
[6] E. Tolosano, S. Fagoonee, N. Morello, F. Vinchi, V. Fiorito, Heme scavenging and the other facets of hemopexin, Antioxid. Redox Signaling 12 (2010) 305–320.
[7] M.R. Mauk, A. Smith, A.G. Mauk, An alternative view of the proposed alternative activities of hemopexin, Protein Sci. 20 (2011) 791–805.
[8] G. Fanali, A. di Masi, V. Trezza, M. Marino, M. Fasano, P. Ascenzi, Human serum albumin: from bench to bedside, Mol. Aspects Med. 33 (2012) 209–290.
[9] U. Muller-Eberhard, K. Grizzuti, Conformational studies on human and rabbit plasma hemopexin and on the effect of ligands on the rabbit heme-hemopexin complex, Biochemistry 10 (1971) 2062–2066.
[10] M. Milani, Y. Ouellet, H. Ouellet, M. Guertin, A. Boffi, G. Antonini, A. Bocedi, M. Mattu, M. Bolognesi, P. Ascenzi, Cyanide binding to truncated hemoglobins: a crystallographic and kinetic study, Biochemistry 43 (2004) 5213–5221.
[11] D. de Sanctis, P. Ascenzi, A. Bocedi, S. Dewilde, T. Burmester, T. Hankeln, L. Moens, M. Bolognesi, Cyanide binding and heme cavity conformational transitions in *Drosophila melanogaster* hexacoordinate hemoglobin, Biochemistry 45 (2006) 10054–10061.
[12] A. Bolli, C. Ciaccio, M. Coletta, M. Nardini, M. Bolognesi, A. Pesce, M. Guertin, P. Visca, P. Ascenzi, Ferrous *Campylobacter jejuni* truncated hemoglobin P displays an extremely high reactivity for cyanide: a comparative study, FEBS J. 275 (2008) 633–645.
[13] D.O. Lambeth, G. Palmer, The kinetics and mechanism of reduction of electron-transfer proteins and other compounds of biological interest by dithionite, J. Biol. Chem. 248 (1973) 6095–6103.
[14] H. Bateman, Solution of a system of differential equations occurring in the theory of radio-active transformations, Proc. Cambridge Philos. Soc. 15 (1910) 423–427.
[15] M. Paoli, B.F. Anderson, H.M. Baker, W.T. Morgan, A. Smith, E.N. Baker, Crystal structure of hemopexin reveals a novel high-affinity heme site formed between two beta-propeller domains, Nat. Struct. Biol. 6 (1999) 926–931.
[16] A.A. Schaffer, L. Aravind, T.L. Madden, S. Shavirin, J.L. Spouge, Y.I. Wolf, E.V. Koonin, S.F. Altschul, Improving the accuracy of PSI-BLAST protein database searches with composition-based statistics and other refinements, Nucleic Acids Res. 29 (2001) 2994–3005.
[17] D. Petrey, Z. Xiang, C.L. Tang, L. Xie, M. Gimpelev, T. Mitros, C.S. Soto, S. Goldsmith-Fischman, A. Kernytsky, A. Schlessinger, I.Y. Koh, E. Alexov, B. Honig, Using multiple structure alignments, fast model building, and energetic analysis in fold recognition and homology modelling, Proteins 53 (Suppl. 6) (2003) 430–435.
[18] M. Antonini, Brunori, Hemoglobin and Myoglobin in Their Reactions With Ligands, North Holland Publishing Co., Amsterdam, 1971.
[19] M. Brunori, M. Coletta, P. Ascenzi, M. Bolognesi, Kinetic control of ligand binding processes in hemoproteins, J. Mol. Liq. 42 (1989) 175–193.
[20] M. Bolognesi, D. Bordo, M. Rizzi, C. Tarricone, P. Ascenzi, Nonvertebrate hemoglobins: structural bases for reactivity, Prog. Biophys. Mol. Biol. 68 (1997) 29–68.
[21] G.M. Giacometti, P. Ascenzi, M. Brunori, G. Rigatti, G. Giacometti, M. Bolognesi, Absence of water at the sixth co-ordination site in ferric *Aplysia* myoglobin, J. Mol. Biol. 151 (1981) 315–319.
[22] M. Bolognesi, S. Onesti, G. Gatti, A. Coda, P. Ascenzi, M. Brunori, *Aplysia limacina* myoglobin: crystallographic analysis at 1.6 Å resolution, J. Mol. Biol. 205 (1989) 529–544.
[23] E. Conti, C. Moser, M. Rizzi, A. Mattevi, C. Lionetti, A. Coda, P. Ascenzi, M. Brunori, M. Bolognesi, X-ray crystal structure of ferric *Aplysia limacina* myoglobin in different liganded states, J. Mol. Biol. 233 (1993) 498–508.
[24] J. Mintorovitch, D. van Pelt, J.D. Satterlee, Kinetic study of the slow cyanide binding to *Glycera dibranchiata* monomer hemoglobin components III and IV, Biochemistry 28 (1989) 6099–6104.
[25] A. Brancaccio, F. Cutruzzolà, C. Travaglini Allocatelli, M. Brunori, S.J. Smerdon, A.J. Wilkinson, Y. Dou, D. Keenan, M. Ikeda-Saito, R.E. Brantley Jr., J.S. Olson, Structural factors governing azide and cyanide binding to mammalian metmyoglobins, J. Biol. Chem. 269 (1994) 13843–13853.
[26] N.C. Veitch, Horseradish peroxidase: a modern view of a classic enzyme, Phytochemistry 65 (2004) 249–259.
[27] S. Herold, A. Fago, R.E. Weber, S. Dewilde, L. Moens, Reactivity studies of the Fe(III) and Fe(II)NO forms of human neuroglobin reveal a potential role against oxidative stress, J. Biol. Chem. 279 (2004) 22841–22847.
[28] F. Viola, S. Aime, M. Coletta, A. Desideri, M. Fasano, S. Paoletti, C. Tarricone, P. Ascenzi, Azide, cyanide, fluoride, imidazole and pyridine binding to ferric and ferrous native horse heart cytochrome *c* and to its carboxymethylated derivative: a comparative study, J. Inorg. Biochem. 62 (1996) 213–222.
[29] R. Varhač, N. Tomášková, M. Fabián, E. Sedlák, Kinetics of cyanide binding as a probe of local stability/flexibility of cytochrome *c*, Biophys. Chem. 144 (2009) 21–26.
[30] S. Dupré, M. Brunori, M.T. Wilson, C. Greenwood, Kinetics of carbon monoxide binding and electron transfer by cytochrome *c* polymers, Biochem. J. 141 (1974) 299–304.
[31] E. Olivas, D.J. De Waal, R.G. Wilkins, Reduction of metmyoglobin derivatives by dithionite ion, J. Biol. Chem. 252 (1977) 4038–4042.
[32] E. Antonini, P. Ascenzi, M. Bolognesi, E. Menegatti, M. Guarneri, Transient removal of proflavine inhibition of bovine β-trypsin by the bovine basic pancreatic trypsin inhibitor (Kunitz): a case for "chronosteric effects", J. Biol. Chem. 258 (1983) 4676–4678.
[33] D. Job, B. Zeba, A. Puppo, J. Rigaud, Kinetic studies of the reaction of ferric soybean leghemoglobins with hydrogen peroxide, cyanide and nicotinic acid, Eur. J. Biochem. 107 (1980) 491–500.
[34] M. Nardini, C. Tarricone, M. Rizzi, A. Lania, A. Desideri, G. De Sanctis, M. Coletta, R. Petruzzelli, P. Ascenzi, A. Coda, M. Bolognesi, Reptile heme protein structure: X-ray crystallographic study of the aquo-met and cyano-met derivatives of the loggerhead sea turtle (*Caretta caretta*) myoglobin at 2.0 Å resolution, J. Mol. Biol. 247 (1995) 459–465.
[35] A. Bellelli, G. Antonini, M. Brunori, B.A. Springer, S.G. Sligar, Transient spectroscopy of the reaction of cyanide with ferrous myoglobin: effect of distal side residues, J. Biol. Chem. 265 (1990) 18898–18901.
[36] R.P. Cox, M.R. Hollaway, The reduction by dithionite of Fe(III) myoglobin derivatives with different ligands attached to the iron atom: a study by rapid-wavelength-scanning stopped-flow spectrophotometry, Eur. J. Biochem. 74 (1977) 575–587.
[37] A. Boffi, A. Ilari, C. Spagnuolo, E. Chiancone, Unusual affinity of cyanide for ferrous and ferric *Scapharca inaequivalvis* homodimeric haemoglobin: equilibria and kinetics of the reaction, Biochemistry 35 (1996) 8068–8074.
[38] W.D. Ellis, H.B. Dunford, The kinetics of cyanide and fluoride binding by ferric horseradish peroxidase, Biochemistry 7 (1968) 2054–2062.
[39] C. Phelps, E. Antonini, M. Brunori, The binding of cyanide to ferroperoxidase, Biochem. J. 122 (1971) 79–87.
[40] E.F. Pettersen, T.D. Goddard, C.C. Huang, G.S. Couch, D.M. Greenblatt, E.C. Meng, T.E. Ferrin, UCSF Chimera: a visualization system for exploratory research and analysis, J. Comput. Chem. 25 (2004) 1605–1612.